Geophys. J. Int. (2007) **169,** 579–592 doi: 10.1111/j.1365-246X.2007.03336.x

The 2003 M_W 7.2 Fiordland subduction earthquake, New Zealand: aftershock distribution, main shock fault plane and static stress changes on the overlying Alpine Fault

Peter McGinty* and Russell Robinson

GNS Science, PO Box 30368 *Lower Hut, New Zealand. E-mail: r.robinson@gns.cri.nz*

Accepted 2006 December 15. Received 2006 December 14; in original form 2006 January 26

SUMMARY

The 2003 August 21 Fiordland earthquake (M_L7.0, M_W7.2) was the largest earthquake to occur in New Zealand for 35 yr and the fifth of M6+ associated with shallow subduction in Fiordland in the last 15 yr. The aftershocks are diffuse and do not distinguish between the two possible main shock fault planes implied by the Harvard CMT solution, one corresponding to subduction interface thrusting and the other corresponding to steeply seaward dipping thrusting. The distinction is important for calculating the induced stress changes on the overlying Alpine Fault which has a history of very large earthquakes, the last possibly in 1717. We have relocated the aftershocks, using data from temporary seismographs in the epicentral region and the double difference technique. We then use the correlation between aftershock hypocentres and regions of positive changes in Coulomb Failure Stress (CFS) due to various candidate main shock fault planes to argue for concentrated slip on the shallow landward dipping subduction interface. Average changes in CFS on the offshore segments of the Alpine Fault are then negative, retarding any future large events. In our models the change in CFS is evaluated on faults of optimal orientation in the regional stress field as determined by inversion of *P*-wave polarities.

Key words: aftershocks; Alpine Fault, Fiordland, induced stress, New Zealand, stress inversion.

INTRODUCTION

Fiordland is a remote, highly active seismic region in the southwest of the South Island of New Zealand (Fig. 1) where oblique convergence between the Australian and Pacific plates occurs. Plate convergence at a rate of 34 mm yr^{-1} and azimuth of 62° (DeMets *et al.* 1994) is accommodated by the Australian Plate being subducted perpendicular to the margin (strike ∼30°) and by strike-slip parallel to the margin on overlying faults, primarily the offshore extension of the Alpine Fault. Deep events associated with the subducted plate extend to depths of 150 km. (Eberhart-Phillips & Reyners 2001).

The 2003 August 21 Fiordland earthquake (M_L7.0, M_W7.2) was the largest shallow earthquake to occur in New Zealand for 35 yr and the fifth with a magnitude M_W 6.0 or greater to occur in the Fiordland region in a 15 yr period (Reyners *et al.* 2003). The Harvard and USGS moment tensor solutions are consistent with a thrust event on the shallow plate interface. Previous earthquakes in the region include: Te Anau, 1988, M_W 6.7, depth 60 km; Doubtful Sound, 1989, M_W 6.4, depth 24 km; Secretary Island, 1993, M_W 6.8, depth 22 km; Thompson Sound, 2000, M_W 6.1, depth 18 km (Fig. 1). The 1988 Te Anau earthquake was interpreted by Reyners *et al.* (1991) as tearing along dip of the subducted slab at depth. The other earthquakes occurred at much shallower depths and are related to plate convergence rather than to the internal stresses in the subducted plate. Reyners & Webb (2002) interpreted both the Doubtful Sound and Secretary Island earthquakes as thrusting on the plate interface. However, Robinson *et al.* (2003) in their study of the Thompson Sound event relocated the Doubtful Sound and Secretary Island sequences as well, using the double difference location method of Waldhauser & Ellsworth (2000). They concluded that both the Doubtful Sound and Thompson Sound earthquakes were oblique thrust events above the plate interface.

In addition to subduction associated earthquakes, the seismic hazard in the region is increased by the offshore section of the predominantly dextral strike-slip Alpine Fault. which has the potential to produce earthquakes of the order of magnitude eight (Stirling *et al.* 2002; Barnes *et al.* 2005; Sutherland *et al.* 2007). The Alpine Fault extends on land to the northeast for 480 km, almost the entire length of the South Island of New Zealand. The most recent major earthquake to occur on the on land sections was in 1717 when the rupture extended over a distance of at least 375 km (Wells *et al.* 1999). Such events are thought to have an average recurrence time of ∼240 yr (Norris & Cooper 2001; Rhoades & Van Dissen 2003) but with a wide variation (Robinson 2004). The offshore section of the

*Now at: Statistics New Zealand. P.O. Box 2922, Wellington, New Zealand.

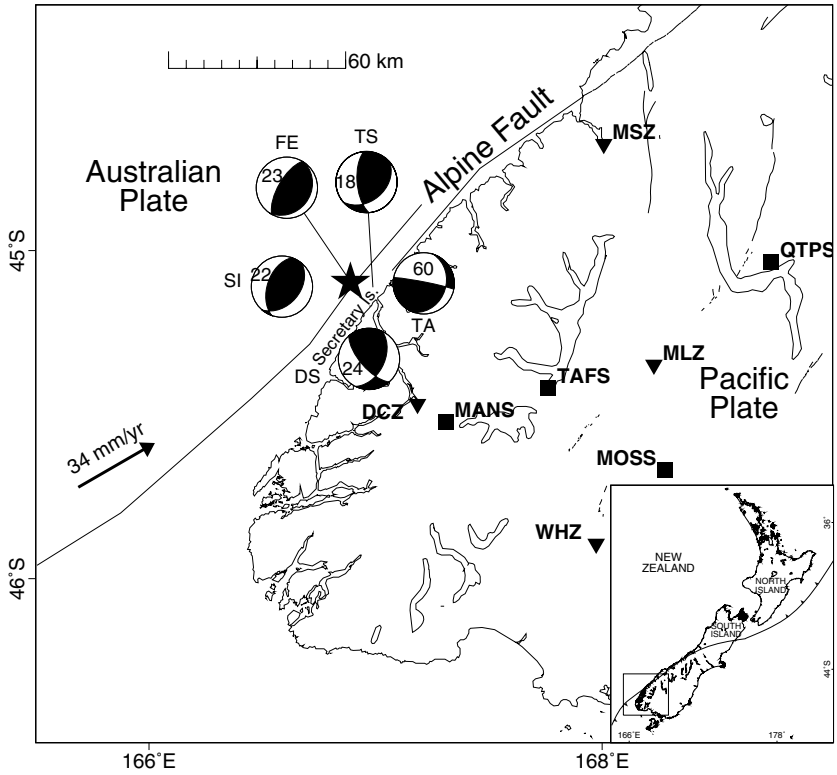

Figure 1. The Fiordland region, southwest South Island, New Zealand. The star represents the epicentre of the 2003 Fiordland earthquake. Focal mechanisms (lower hemisphere) are shown at the epicentres of the Te Anau (TA: 1988, M_w 6.7 and depth 60 km), Doubtful Sound (DS: 1989, M_w 6.4 and depth 24 km), and Secretary Island (SI: 1993, M_w 6.8 and depth 22 km) events. The mechanisms of the Thompson Sound (TS: 2000, M_w 6.1) and present Fiordland (FE: 2003, M_w 7.2) events are also shown, but displaced from their epicentres joined by a line. DS also indicates the entrance to Doubtful Sound south of Secretary Island. Four of the nearby permanent National Seismograph Network stations (MSZ, DCZ, MLZ and WHZ) are shown by triangles. Four of the nearby permanent National Strong-motion Network stations (MANS, TAFS, MOSS and QTPS) are shown by squares. The two main traces of the Alpine Fault are shown by a solid line (interpreted from Barnes *et al.* 2005). The arrow indicates the direction of plate convergence at 34 mm yr^{-1}.

Alpine Fault extends for several hundred kilometres southwest from Milford Sound (MSZ, Fig. 1), but the last date of rupture is not known so it could be that events such as that in 1717 extend offshore as well. In the Fiordland region the strike of the offshore Alpine Fault differs from the azimuth of plate convergence by 11°–25°; so pure strike slip events on it would still leave a smaller component of convergence perpendicular to the coast to be taken up elsewhere.

Besides its intrinsic interest, it is important to determine as precisely as possible the geometry of the 2003 Fiordland main shock fault plane, and its mechanism, given the importance of large earthquakes bringing forward or retarding large events on other nearby faults (Harris 1998; King & Cocco 2001; McCloskey *et al.* 2005). Teleseismic focal mechanisms cannot tell which nodal plane is the actual fault plane. Thus following the 2003 Fiordland earthquake, a temporary network of six portable seismographs and four strong-motion instruments was deployed in the region (Fig. 2) to supplement the New Zealand National Seismological Network. 8025 aftershocks were recorded up until 2003 October 31, including 23 earthquakes of magnitude 5.0 or greater. Many near-source strong motion records were collected, including one with 28 per cent g peak-ground-acceleration from the largest aftershock (magnitude M_L 6.1, M_W 5.5) at an epicentral distance of only a few km (Reyners *et al.* 2003; McGinty 2004). Recordings at such close distances are rare in New Zealand.

Although one nodal plane of the Harvard teleseismic focal mechanism matches the plate interface, parallel to the coast and dipping landward (SE), routine locations of aftershocks (Fig. 2) define a very diffuse zone of activity not clearly associated with the plate interface. In fact they, in part, could vaguely suggest a main shock rupture plane dipping steeply seaward (NW), corresponding to the other nodal plane. In this study, we relocate earthquakes associated with the Fiordland 2003 sequence using the same velocity model and double difference procedure that were used in the Thompson Sound study of Robinson *et al.* (2003), so that a direct comparison between sequences can be made. We then compare these relocations to regions of increased Coulomb Failure Stress (CFS) due to slip on main shock fault planes corresponding to the two nodal plane orientations. The hope is that one or the other will be clearly preferable. To do this we need the background stress orientation in the region, obtained by the inversion of *P*-wave polarities from the better located events. With the main shock fault plane identified, we can then examine the effect that the Fiordland earthquake had on the offshore section of the Alpine Fault, via induced static stress changes.

Note that while the main shock epicentre is near Secretary Island (Figs 1 and 2), to avoid confusion with an earlier event in 1993, the present main shock is referred to as the 2003 Fiordland event.

AFTERSHOCK DATA

To enhance the aftershock recording coverage in the epicentral region and complement the New Zealand National Seismic Network (NZNSN), 10 portable instruments were deployed in the 3 d following the 2003 Fiordland earthquake (DCZ and insert, Fig. 2). The

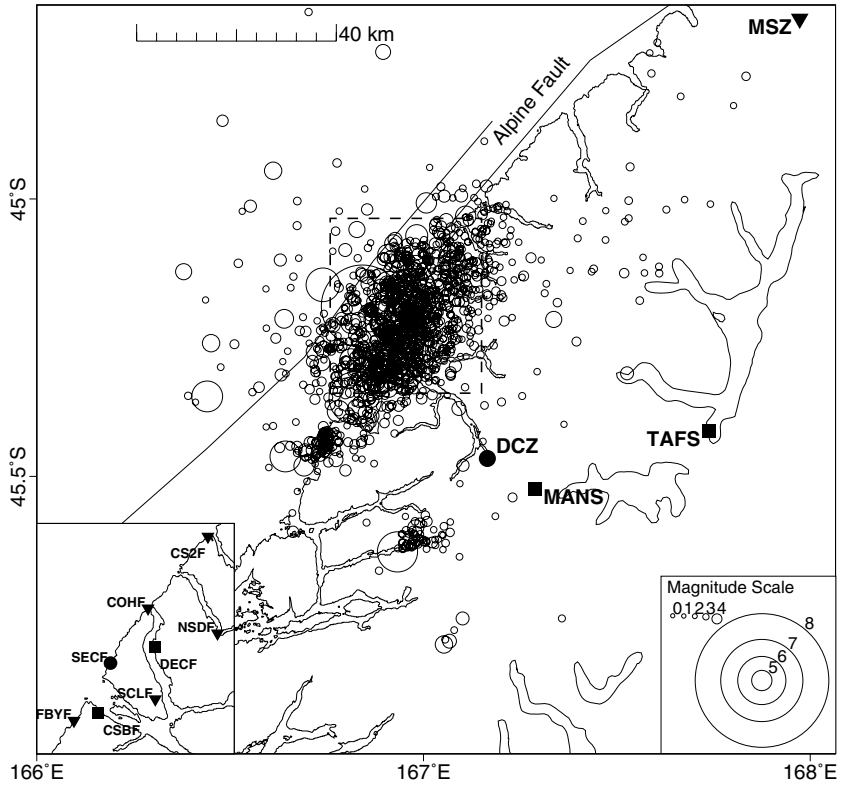

Figure 2. Circles represent the epicentres of earthquakes with magnitude three or greater recorded between 2003 August 21 and October 31. Symbol size is proportional to magnitude. The two lines off shore paralleling the coast represent the Alpine Fault. Insert shows the location of the portable short-period (triangles and circle) and strong-motion (squares and circle) network. Also shown are nearby national network stations with instrumentation symbolized as for the portable stations.

main shock occurred near the coast of a road-less part of the South Island of New Zealand, 60 km from the nearest town, Te Anau (TAFS, Figs 1 and 2). The terrain there is heavily vegetated and extremely rough, and dissected by deep fiords. As a consequence, access to the aftershock zone area was by helicopter. From the air many landslides were observed and mapped (Reyners *et al.* 2003; Hancox *et al.* 2004).

In the first half hour of operation the short period instrument at SECF recorded 10 aftershocks with a typical *S–P* time of 2.5 s, indicating that this site was very close to the epicentres if they were occurring at about the depth of the plate interface (∼25 km). It should be noted that because of high winds and proximity to the very stormy coast, the portable instruments operated at relatively low gains.

All but two of the portable instruments were retrieved on September 15 after about 3 weeks of being in the field. It was decided to add solar panels to the portable short period instruments at SECF and CSDF and leave them in the field. However, when the CSDF site (∼20 m above sea level) was revisited the instrument was found to be completely full of sea water and no data were retrievable. A replacement site for CSDF was found slightly inland and at a higher elevation. These sites were removed in 2004 May.

All data from the portable instruments were added to data from the permanent stations and processed using the standard New Zealand earthquake location method to obtain preliminary locations and magnitudes. For the period considered here for relocating events, 2003 August 21 to October 31, 8025 events were located in or near the aftershock zone, with magnitudes (M_L) from 1.0 to 6.1.

EARTHQUAKE RELOCATION PROCESS

Earthquake locations reported in the routine New Zealand earthquake catalogue have been obtained using the standard New Zealand crustal velocity model, which is an average 1-D model for the whole of New Zealand and does not take into account any regional variation. It consists of two crustal layers of thickness 12 and 21 km over a half-space mantle, V_p of 5.5, 6.5 and 8.05 km s^{-1} and V_p/V_s of 1.73. The deployment of portable seismic instruments following the 2003 Fiordland and other recent Fiordland earthquakes, along with past passive seismic surveys in the region (Eberhart-Phillips & Reyners 2001), have provided the data to obtain a more appropriate velocity model for the region.

Eberhart-Phillips & Reyners (2001) determined both a 1-D and a 3-D velocity model for the Fiordland region using data from a 3 month deployment (30 km average spacing) in 1993, a 6 month deployment in late 1995 and early 1996, and aftershocks from the 1993 M_W 6.9 Secretary Island earthquake. The 3-D model, however, is not well constrained near the coast or offshore. To obtain good relative locations for the 2003 Fiordland earthquake sequence we use the double difference method of Waldhauser & Ellsworth (2000) and the 1-D velocity model of Eberhart-Phillips & Reyners (2001). We also use the same parameters (available from the authors) as Robinson *et al.* (2003) in the double difference procedure, so that a direct comparison of our results with theirs can be done. Menke & Schaff (2004) argued that double difference locations are good not just for relative positions, but also absolute positions. We have not used cross-correlations to get relative times; in our case tests show that there is very little additional improvement.

Table 1a. Location quality criterion.

Quality	A	B	C	D	F
Distance to nearest station (km)	≤Depth	≤2*Depth	≤3*Depth	>3*Depth	>3*Depth
Number of stations	≥6	≥5	≥4	3	3
rms traveltime residual (s)	≤0.10	≤0.15	≤0.25	≤0.50	>0.50
Number of phases	≥8	≥6	≥5	≥4	4
Convergence	Yes	Yes	Yes	Yes	No
S.E. of X and Y (km)	≤0.5	≤1.0	≤1.5	>1.5	>1.5
S.E. of depth (km)	≤1.0	≤2.0	≤3.0	>3.0	>3.0
S.E. of origin time	≤0.05	≤0.10	≤0.15	>0.15	>0.15
At least one *S* phase	Yes	Yes	Yes	No	No

Table 1b. Average formal location errors.

Quality	A	B	C	D	F
Average *E* error (km)	0.21	0.38	0.57	1.16	0.59
Average *N* error (km)	0.23	0.41	0.66	1.42	0.91
Average depth error (km)	0.21	0.40	0.65	1.85	0.92
Average origin time error (s)	0.04	0.07	0.11	0.22	0.26

To prepare the data for the double difference procedure we use the Eberhart-Phillips & Reyners (2001) 1-D velocity model but invert for *P* and *S* station corrections for both the portable and nearby (<200 km) national network stations, using the Fiordland data itself. We also fix the *P* term of the portable station on Secretary Island (SECF) to zero. For an earthquake to be included in the data set it had to have been recorded by at least seven stations with *P* weights of 100 or 75 per cent and at least two *S* readings of 50 per cent or better. The inversion was iteratively repeated after removing arrivals with large traveltime residuals or entire events if a removal of an arrival meant the above criteria was not met. In the end, 364 earthquakes were used in the final inversion set.

Station terms determined in the inversion and the 1-D velocity model of Eberhart-Phillips & Reyners (2001) were then used to relocate all the earthquakes with the location program Loc1d (Robinson 1994). This was done to obtain good starting locations for the double difference procedure and determine the quality of each earthquake hypocentre. Each relocated earthquake had to have been recorded at a minimum of five stations for which station terms were available. Each earthquake was classified in terms of location quality (A, B, C and D; Table 1a, Robinson 1994) and the types of stations included in its location. If there were a sufficient number (5) of portable stations, along with DCZ and MANS, then the location was 'L' (Local) type and only those stations were used. Otherwise the location was 'D' (Distant) type and all stations that directly contributed to the inversion were used. Table 2 shows the numbers of events in the various data sets used in this study. Table 1b shows the average formal mislocation errors for the various qualities. We think that the use of *S* phases and a local velocity model reduce the possibility of large systematic location errors compared to *P* only solutions.

SPATIAL DISTRIBUTION OF RELOCATED EARTHQUAKES

To examine the distribution of events in the 2003 Fiordland earthquake sequence we first examine all 1771 double difference locations, regardless of initial quality, including the main shock (Quality D in Table 1). These are shown in map view and cross-section in Fig. 3. The primary feature of the locations, in map view, is an intense region of activity near the coast, or just offshore, striking northeast and ∼50 km long. In addition, there are four distinctly separate clusters of activity: (1) 15 km to the southwest (SW), (2) 35 km to the south (S1), (3) 60 km to the south (S2) and (4) 30 km to the east (E). The first two subclusters have associated with them a 'main shock' (SW, M_W 5.4 on 2003 August 26; S1, M_W 5.6 on 2003 September 30) that initiated the remaining activity. Events in the eastern subcluster are within the deeper part of the subducted plate at depths of 80–130 km.

In cross-section (Fig. 3b), the main region of activity forms a diffuse cloud, dipping vaguely to the southeast, at depths mainly between 10 and 27 km, with an indication of a more active deeper section to the southeast, and a shallower less active section to the northwest. Depths of events in the SW and the two southern clusters, not shown in the cross-section, are mainly between 20 and 27, 10 and 18 and ∼25 km, respectively. The less numerous but better relocations (double-difference quality A, B and C, L type locations, Table 2) give a better resolution picture of the main aftershock zone and the subcluster to the southwest (Fig. 4a). This data does not include the main shock. The length of the main zone now appears to be ∼40 km, with a width of ∼12 km, and overall strike between 25° and 30°. There is a hint however that the strike is more easterly to the north, more northerly to the south. The main body of aftershocks in cross-section (Fig. 4b) shows that it is made up of two distinct groups. The shallower, northwest, group is concentrated more to the north end of the aftershock zone (Fig. 4c). The bigger events are located around the deeper, southeast cluster. Not included in the cross-sections are events from the subclusters previously identified. Events in the close, southwest subcluster, SW, form a tightly bunched group centred at about 25 km depth. In the closest cluster to the south, S1, events define a southeast dipping fault plane in the depth range 10–20 km, with the largest event in this group near the top of the fault. This apparent fault plane is close to one of the focal planes in the Harvard CMT solution for its 'main shock', M_W 5.6. (Table 3).

Aftershock distributions sometimes define a clear main shock rupture plane, but no obvious fault plane is evident from the distribution of the better quality events. Fig. 4(b) shows the events projected onto a vertical plane perpendicular to the strike of the subduction zone (35°) and the same orientation used by Robinson *et al.* (2003). From the location of the aftershocks alone, many fault plane orientations could be suggested, none with any particularly strong case. Neither of the two focal planes in the Harvard CMT solution for the main shock (Table 3) appears to be matched by the aftershock distribution, except for the strike. The aftershock 'cloud' does, however, lie on the position of the plate interface suggested by

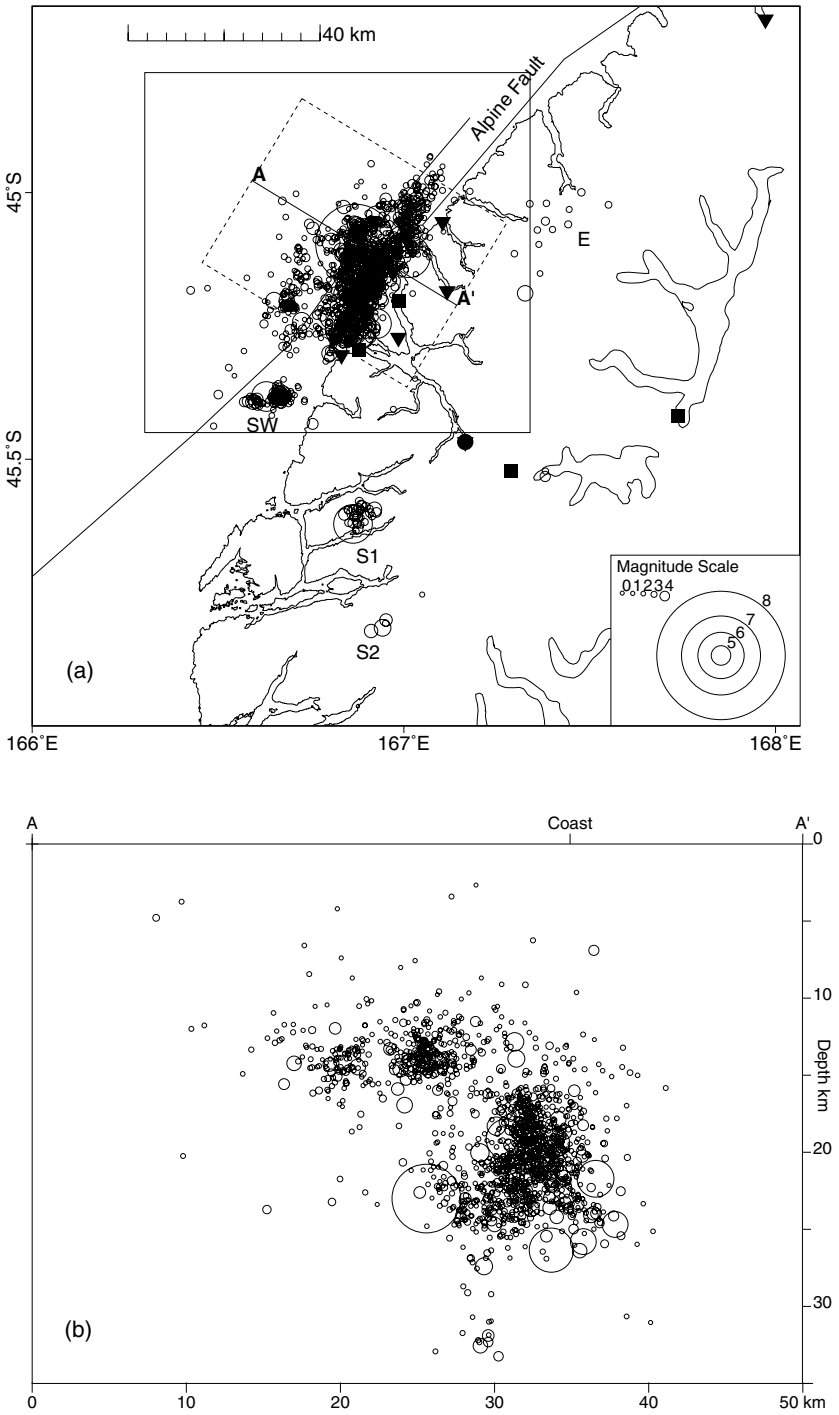

Figure 3. All 1770 double-difference relocated 2003 Fiordland earthquakes, regardless of initial quality, including the main shock. Symbol size is proportional to magnitude. (a) Map view, with station positions (stations closest to the aftershock are obscured, see Fig. 2). The box indicates the area shown in Figs 4(a), 5(a) and 6(a). (b) Cross-section A–A′.

background seismicity recorded during a 3 month deployment of portable instruments in 1993 (Eberhart-Phillips & Reyners 2001) (true to seismological tradition these instruments were removed shortly before the 1993 Secretary Island main shock).

When the double-difference locations of previous aftershock sequences are compared to the 2003 sequence (Fig. 5), it is found that the 1993 Secretary Island sequence overlaps the shallower, northwest group of the present 2003 sequence, but extends further southwest. We can thus interpret the latter events as marking the partial reactivation of the 1993 event's aftershock zone. The 1993 sequence also has a cluster of events further offshore which were interpreted by Reyners & Webb (2002) as outer rise events as typically found at subduction zones. We note here that the 2003 Fiordland sequence has no outer-rise events. The 2000 Thompson Sound aftershock sequence lies mainly to the northeast of the 2003 sequence, and above the deeper southeast group.

Table 2. Number of events used in various data sets of aftershock of the 2003 Fiordland earthquake.

21/08/03–31/10/03	Total number of events	Quality		
		AL	BL	CL
Catalogue	8025	–	–	–
Local velocity model + station terms (Loc1d)	1809	38	229	111
Double-differenced	1771	38	228	111

AL = Quality A, using only local stations; BL = Quality B, using only local stations; CL = Quality C, using only local stations.

FOCAL MECHANISMS

Harvard CMT solutions

Harvard CMT solutions are available for four of the events considered in this study (Table 3). They include the main shock and three aftershocks, the last being the 'main shock' of the first southern subcluster S1. With the exception of the last, which has a normal faulting mechanism, the others have similar reverse faulting mechanisms differing only by a slight rotation. The strike of the main shock focal planes matches the observed strike of the aftershock zone; one focal plane has a shallow dip to the southeast suggesting slip on the plate interface. However, as mentioned above, neither plane is particularly evident in the aftershock distribution as seen in cross-section. The normal faulting mechanism of the last event is consistent with the mechanisms determined by Reyners *et al.* (2002) for shallower events on the Fiordland mainland, probably reflecting the uplifting process that has exposed deep crustal rocks in the region.

Aftershock mechanisms

We used the programs AMPRAT and MECHTOOL (Robinson & Webb 1996; Robinson & McGinty 2000) for aftershock focal mechanism analysis. These programmes use primarily first motion data but constraints are provided by a variety (up to seven) of *P*/*S* amplitude ratios. Theoretical ratios are calculated using 1-D synthetic seismograms. We determined focal mechanisms for quality A and B, L type events only (Fig. 6a). The quality of location is important as the focal mechanisms are dependent on accurate ray take-off angles and azimuths. We used only the amplitude ratios from the five short-period portable stations and the NZNSN stations DCZ and MSZ as the other NZNSN stations are too far away (>75 km) for the reliable calculation of the synthetic seismograms. First motion data from the five portable short period instruments, the four NZNSN stations DCZ, MLZ, MSZ, WHZ and four digital Etna strong motion instruments CSBF and DECF (portables), MANS and TAFS (permanent) when available were used. Events had to have amplitude data for all three components of the five portable short period stations and at least seven clear first motion readings. The correlation between observed and calculated amplitude ratios had to be over 0.7. We find that for our data set the above criteria are adequate.

Despite the selection of the best located aftershocks, we feel that the mechanisms are only loosely constrained because of the small amount of data. There are also questions about possible errors in the take-off angles because of unmodelled effects such as propagation along high contrast velocity discontinuities (Ben-Zion & Malin 1991; Hardebeck & Shearer 2003). The synthetic seismograms used to calculate theoretical amplitude ratios may not be very realistic because they are based on a 1-D velocity model.

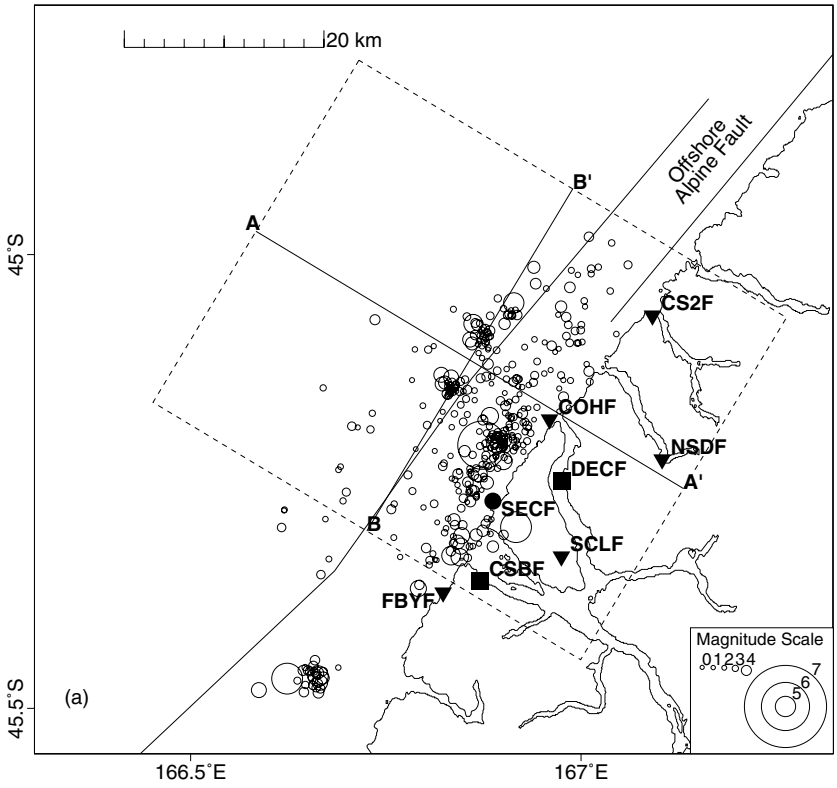

Figure 4. 377 double-difference relocated 2003 Fiordland aftershocks using the best quality initial locations (see text). The two strait lines indicate the approximate position of two branches of the Alpine Fault as used for induced stress calculations. (a) Map view. (b) Cross-section A–A′. (c) Cross-section B–B′′.

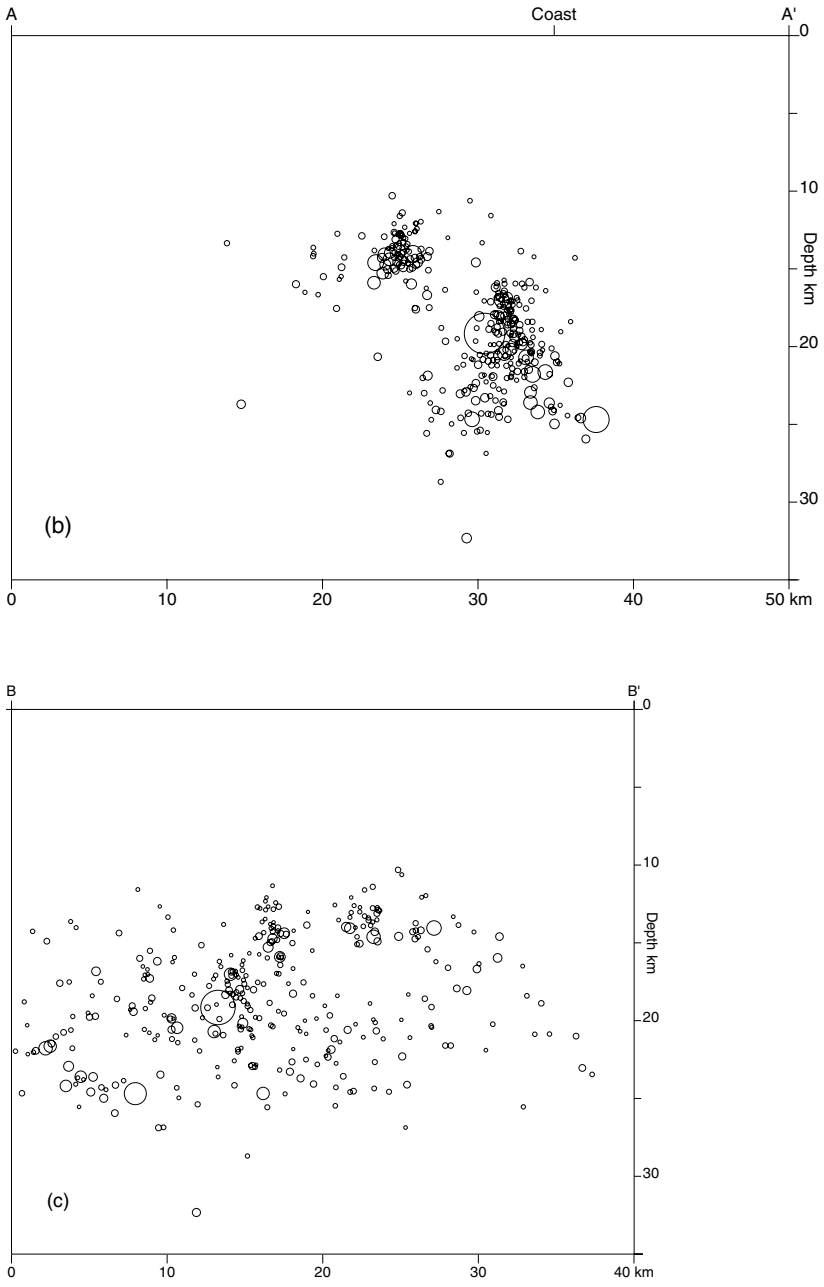

Figure 4. (*Continued.*)

Table 3. Harvard CMT solutions for Fiordland earthquakes (2003 August and September).

Harvard CMT date (M_w)	Fault	Strike (°)	Dip (°)	Rake (°)	Depth (km)	Moment (Nm)
2003/08/21 (7.2)	1	35	23	95	31.8	7.48×10^{20}
	2	209	67	88		
2003/08/26 (5.4)	1	37	36	108	18.0	1.76×10^{18}
	2	196	56	78		
2003/09/04 (5.5)	1	216	24	91	27.3	2.04×10^{18}
	2	35	66	90		
2003/09/30 (5.6)	1	246	27	−113	15.0	2.66×10^{18}
	2	92	65	−78		

Individual focal mechanisms for 35 aftershocks were determined (Fig. 6a). They have a wide range of solutions but as a group their *P*- and *T*-axes have some systematic features (Fig. 6b). The *T*-axes lie in more of a belt suggesting that $\sigma 2$ and $\sigma 3$ are similar in magnitude. We have determined 'averages' (also in Fig. 6b) by finding directions around which the moment of inertia of the individual *P*- and *T*-axes are minimized (Davis 1986). We use this method because the axes are just that, they are not vectors with a direction like magnetic declinations.

DETERMINATION OF THE REGIONAL STRESS TENSOR

Later in this study, we investigate the changes in stress induced by various main shock geometries. In the cases where these stress

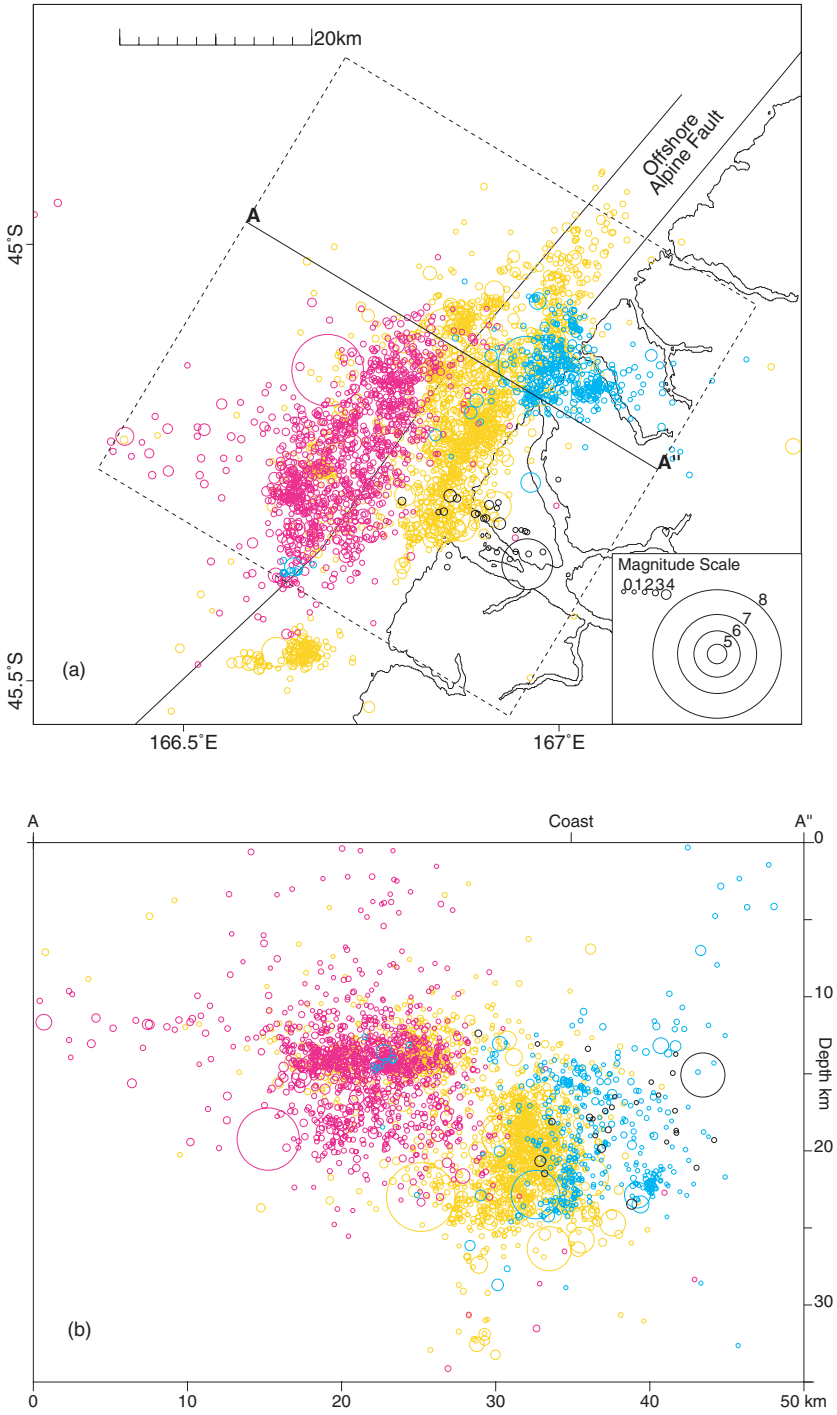

Figure 5. (a) Double-difference relocations of main shock and aftershocks of the 1989 Doubtful Sound (black circles), the 1993 Secretary Island (red circles), the 2000 Thompson Sound (blue circles) and the 2003 Fiordland earthquakes (yellow circles). A–A′ represents the cross-section in (b).

changes are calculated for 'optimally oriented' faults, the regional stress tensor is required. We have used the focal mechanism inversion program of Michael (1987a) with the 35 aftershock mechanism but the 95 per cent confidence limits, from the resampling technique (Michael 1987b), are extremely broad (e.g. over 200° for the $\sigma 3$ azimuth). This result might be expected given the poorly constrained mechanisms and the spread of *P* and *T* axes.

Since the 2003 Fiordland aftershocks apparently do not lie on a single main shock fault plane, they presumably represent failure on optimally oriented (at least on average) small fractures. We can thus use their *P*-wave polarity data to invert for the stress tensor orientation using the method described in Robinson & McGinty (2000). This method does not require individual event mechanisms, but does require a specified coefficient of (dry) friction, 0.7 here. Because data from the numerous small aftershocks (even if only one first motion) are used, the confidence limits are usually much smaller than for a traditional inversion. Broad confidence regions can indicate an inhomogeneous regional stress.

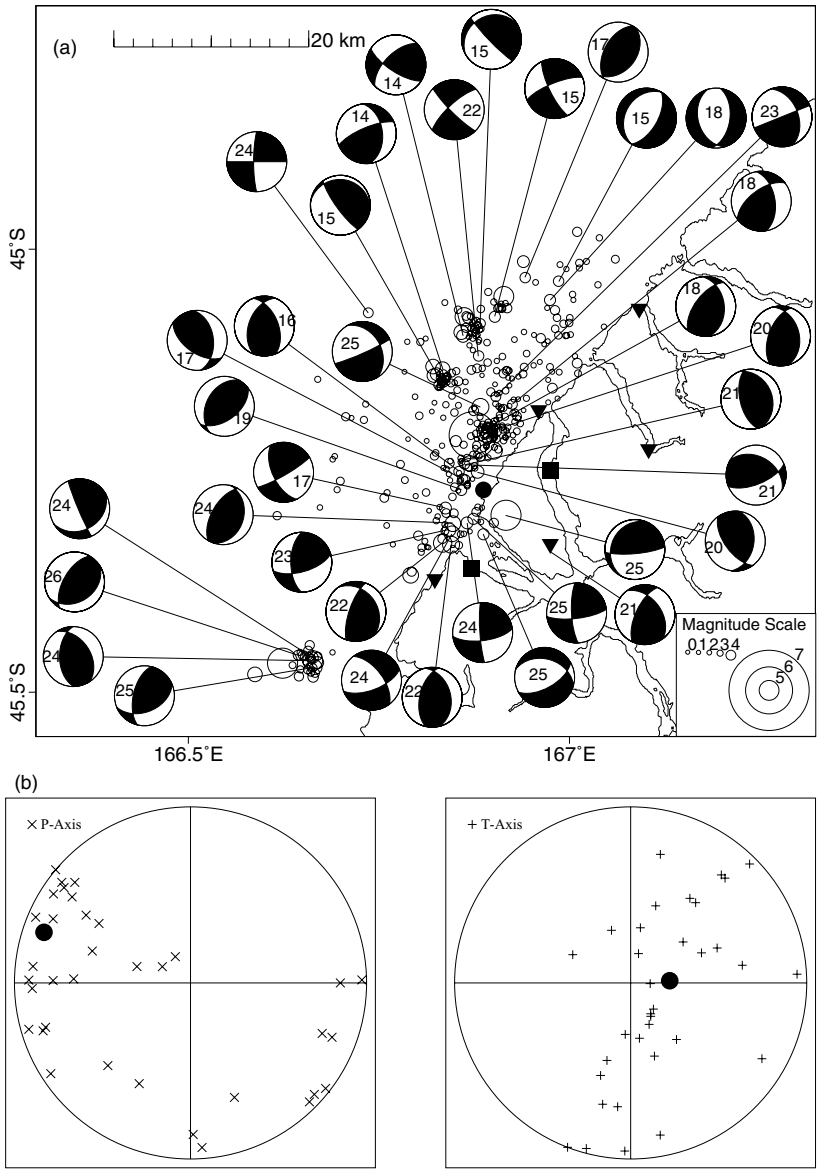

Figure 6. (a) Individual focal mechanisms (lower hemisphere) for QAL and QBL aftershocks with sufficient data of magnitude four or greater. Numbers on focal mechanisms indicate the depth of the event (b) Lower hemisphere stereographic plots of aftershock *P*- and *T*-axes for the mechanisms shown in (a); solid circles are the appropriate 'averages' (see text).

From the better located aftershocks in the primary aftershock zone (Fig. 4) two groups of events stood out, a shallower, northwest group and a more numerous deeper, southeast group. Independent stress inversions were done for each group. All *P*-wave polarity data from quality QAL, QBL and QCL earthquakes were used to invert for each stress tensor orientation; each event had its first motion data re-examined. For the shallower, northwest group 75 events were examined and 489 polarities were used. 95 per cent confidence intervals were determined using the resampling technique (Michael 1987b), with 1000 resamples. For the deeper, southeast group 218 events were examined and 1468 polarities were used, with 500 resamples.

The inversion results are shown in Fig. 7, where each circle represents a lower hemisphere stereographic plot. The big circles shows the σ_1 and σ_3 axes corresponding to the stress tensor solutions. The two beach balls to the right of each big circle are the focal mechanisms that correspond to the two optimal fault planes given by the σ_1 and σ_3 axes. On each mechanism the optimal fault plane is indicated by a bold line. Both inversion results represent predominantly reverse faulting, with the σ_1 and σ_3 axes in reasonable agreement with each other, being relatively rotated about a northeast–southwest axis. The differences thus probably reflect the change in dip of the subducted slab with depth.

For the remainder of this study we adopt a regional stress tensor combing the two results, with extra weight for the result for the more numerous events in the deeper SE cluster, for example, $\sigma 1$ azimuth $=$ 314°, $\sigma 1$ dip $= 9^\circ$, $\sigma 3$ azimuth $= 67^\circ$ and $\sigma 3$ dip 69°. The 95 per cent confidence limits are on the order of 10°.

WHERE WAS THE MAIN SHOCK FAULT PLANE?

We have seen that the aftershock locations of the 2003 Fiordland earthquake do not define the main shock fault plane. It has been well documented that aftershock locations off the main shock fault

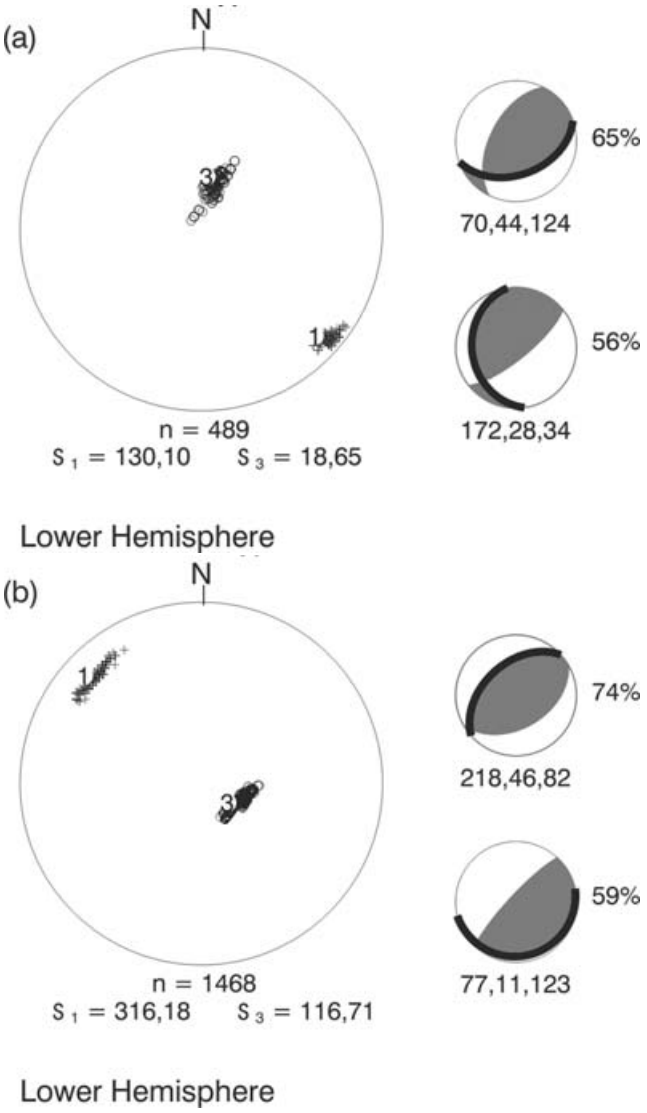

Figure 7. Results of inverting individual *P*-wave polarity observations for a local stress tensor. On the left, '1' indicates the best orientation for the most compressive axis (σ_1) and '3' that for the least (σ_3). The crosses and circles define the 95 per cent confidence limits. On the right are the focal mechanisms (lower hemisphere) that correspond to slip on the two optimally oriented fault planes, giving the strike, dip and rake (the fault plane for each focal mechanism is represented by a bold line). All *P*-wave polarity observations are from QAL, QBL and QCL aftershocks only. (a) Inversion result for the upper cluster of the main body of aftershocks between the depths 10–16 (as in Fig. 4b). (a) Inversion result for the lower cluster of the main body of aftershocks between the depths 16 and 25 (as in Fig. 4b).

plane can be explained by modelling static changes in CFS due to the occurrence of the main shock (Harris 1998; King & Cocco 2001; Das & Henry 2003). We thus adopt an indirect approach by testing different possible main shock fault plane orientations and slip distributions to see how good a correlation between regions of increased CFS and the positions of the aftershocks can be achieved (see McGinty & Robinson 1999, for a similar approach). The changes in CFS are mostly calculated for faults of optimal orientation in the regional stress field. We quantify the 'goodness' of the correlation by determining what percentage of aftershock hypocentres fall in regions of positive changes in CFS, evaluated in 3-D. The same number of random hypocentres (in a volume defined by the latitude, longitude, and depth extent of the real hypocentres) give a percentage of 50 ± 5 per cent in all cases examined. It would be preferable to compare the spatial distribution of increases and deceases in rates of activity before and after the main shock (e.g. Marsan & Nalbant 2005) but this is very difficult because of the much higher magnitude threshold before our portable instruments were installed. Also the location accuracy of the 'before' events is much poorer (often being restricted to a depth of 12 or 33 km) making spatial distinctions impossible.

All induced stress calculations were done using the program GNStress2 (see acknowledgements) which uses the dislocation/strain formulation of Okada (1992) and is thus based on a uniform 3D half-space earth model, with a rigidity of 2.68×10^{10} N m^{-2}.

First we consider one fault 'plane 1' (strike 209°, dip 67° and rake 88°) corresponding to the steeper dipping plane of the Harvard CMT solution; there is some weak suggestion in the deeper SE cluster of aftershock alignment along that trend, when viewed in cross-section (Fig. 4b) and we place the hypothetical main shock plane through that cluster. While normal faults in corresponding regions of other subduction zones are well known, large, sea-ward dipping, thrust faults below the plate interface at shallow depths would be unusual. We take an along-strike length of 60 km and a downdip length of 20 km, with the top of the fault at 15 km depth. To preserve an M_W magnitude of 7.2, it would have an average slip of 2.8 m. Such a main shock is allowed by the available GPS data (John Beavan, personal communication 2006). We use these fault parameters to calculate the change in CFS for optimally oriented faults, and view the results in a cross-section (Fig. 8a) perpendicular to the proposed fault plane (i.e. trending 125°). We find that the percentage of the aftershocks that fall in a region of positive change in CFS (Table 4) is very low, 33.8 per cent (in 3-D, not cross-section). Experiments with a tapered slip distribution or calculating changes of CFS on planes of the same orientation as the main shock, produce even lower correlations. We thus reject this possible main shock fault plane. It is possible to shift the fault horizontally and get a better fit but the required shift is large (>20 km) and no longer consistent at all with GPS observations.

Next we examine the other fault 'plane 2' of the Harvard CMT solution (strike 35°, dip 23° and rake 95°). This is consistent with thrusting on the plate interface. We first describe our preferred model (Table 5) and then examine how well it is constrained.

We restrict the strike to be 35° and the along strike extent to 60 km, the extent of the aftershock epicentres. After much experimentation we find a good fit, 95.2 per cent (Fig. 8b), for a dual segment fault, the dip of the shallower segment being 23° as in the Harvard mechanism, and of the deeper segment being 35°, joining at a depth of 20 km. This is consistent with the interface as delineated by Robinson (2004). Our preferred model extends seaward to a depth of 10 km, remembering that the Alpine Fault must fit in above. In all our trials we found that for best results most of the slip had to be near the hinge line of the two segments, slightly downdip and to the east of the deeper cluster of aftershocks. A simple tapered slip distribution (Fig. 9) works well, and is similar to a teleseismic slip inversion performed by the USGS in the first days after the event (US Geological Survey 2003). To preserve a moment magnitude of 7.2 an average slip of 1 m for both segments is required (equivalent to two magnitudes 7.0 events). This model has good (95.2 per cent) CFS—hypocentre correlation and is also allowed by the available GPS data.

Our main goal has been to distinguish between two quite different main shock fault planes. The results above indicate plane 2 is much more likely given our basic assumptions. A remaining question

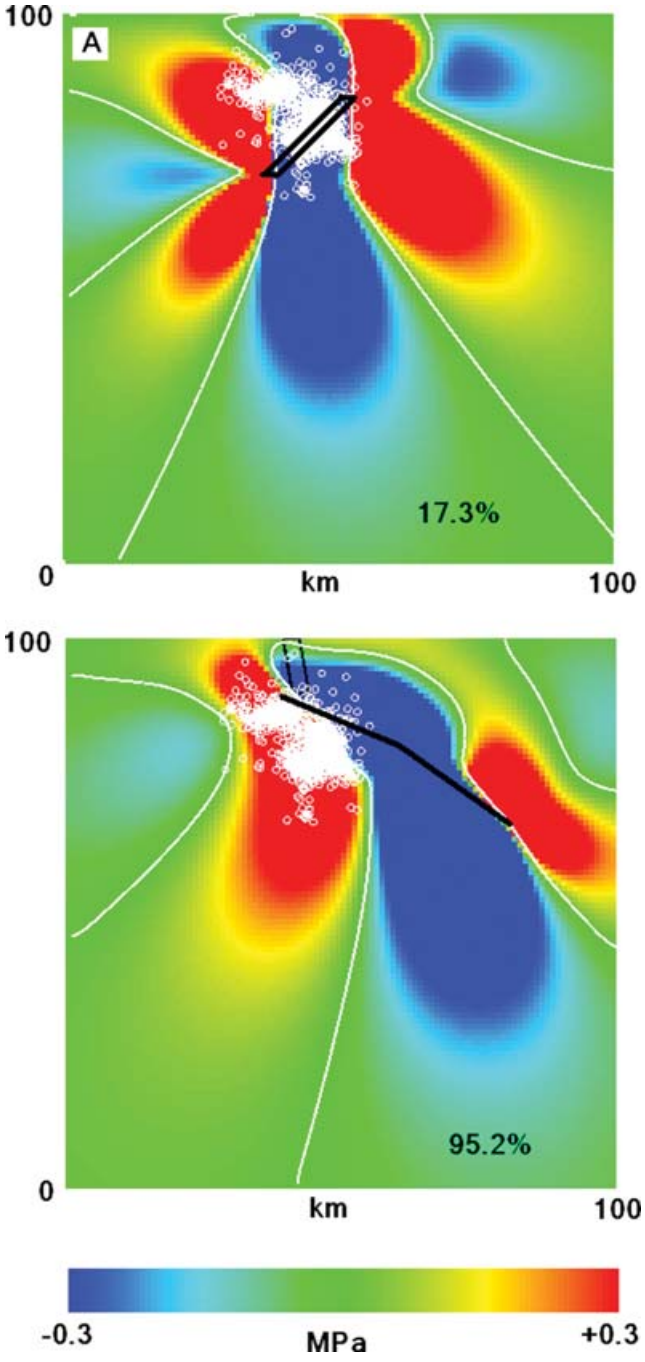

Figure 8. Changes in CFS on optimally oriented faults shown in cross-sections on planes perpendicular to the strike of the model main shock fault planes. The white lines are the zero contours; the white circles are the aftershock hypocentres; the black numbers are the percentage of hypocentres in positive dCFS areas; the bold black lines are the fault planes. (A) For a steeply dipping thrust corresponding to one nodal plane in the Harvard CMT solution, calculated using uniform slip. This view shows that the main body of aftershocks lies within a region of negative change in CFS making it unlikely that the main shock had this orientation. (B) For our preferred fault plane, a hinged system that is reasonably consistent with the other nodal plane of the Harvard CMT, with tapered slip Fig. 9). Note that the southwest cluster of events is not included in this cross-section. The position of the two strands of the Alpine Fault are also shown in black. This view shows that the main body of aftershocks lies within a region of positive change in CFS making it likely that the main shock fault had this orientation, corresponding to thrusting on the plate interface.

Table 4. Percentages of hypocentres in regions of positive changes in CFS, for a main shock fault plane dipping steeply to the NW (plane 1 of Harvard mechanism) and passing through an apparent alignment of hypocentres.

	Percentage in positive region
Tapered slip, dCFS on optimal planes	33.8
Uniform slip, dCFS on optimal planes	17.3
Tapered slip, dCFS on planes like source	29.0
Uniform slip, dCFS on planes like source	14.9

Table 5. Parameters of the preferred model.

	Segment 1	Segment 2
Centre latitude (°)	−45.150	−45.261
Centre longitude (°)	166.960	167.182
Length (km)	60	60
Width (km)	25	25
Top (km)	10	20
Strike (°)	35	35
Dip (°)	23	35
Rake (°)	95	95
Average slip (m)	1.0	1.0
Maximum Slip (m)	2.8	2.8
Cells	10 × 5	10 × 5
Coefficient of friction	0.7	0.7
Initial pore pressure	0.38 × Lithostatic	0.38 × Lithostatic
σ1Azimuth (°)	314.0	314.0
σ1Dip (°)	8.7	8.7
σ3Azimuth (°)	67.0	67.0
σ3Dip (°)	68.6	68.6

is whether or not the good aftershock—CFS correlation for plane 2 would be ruined by some reasonable change in our preferred model, keeping the basic geometry. Table 6 indicates that to substantially reduce the score we would need to use uniform slip, or, to a lesser extent, decrease the coefficient of friction. The coefficient of friction we use is 0.7, based on laboratory and field observations (e.g. Raleigh *et al.* 1972; Brudy *et al.* 1997). It is the dry value. In our model it applies to the small, optimally oriented fault planes which are unlikely to have well developed fault gouge zones. We can see no justification for a lower value. Pore pressure is a separate issue, but it does not change the orientation of the optimal planes and changes only the magnitude of change in CFS, not its sign. Uniform slip is physically unreasonable, and unlikely given the UGS slip inversion results. If we increased the depth of the fault segments, they would no longer correspond to the plate interface, so we regard that as a violation of our basic geometry. Low angle thrusting on some surface well below the plate interface is unlikely. So, we think are preferred model of low angle thrust faulting on the plate interface is well supported.

EFFECT ON THE ALPINE FAULT

Our preferred 2003 Fiordland main shock fault plane can be used to calculate the induced changes in CFS on the overlying Alpine Fault. Here we calculate the change in CFS on the actual Alpine Fault surface itself taken as the nearest two sections of the fault off Secretary Island. The first section is 20 km long and almost parallels most of the length of Secretary Island. It has a strike of 35°, dip of 80° and a rake of −180°. The results for this section (Fig. 10 top) indicate on average a negative change in CFS of −0.37 MPa, with increases mainly confined to shallow depths of a few km, peaking

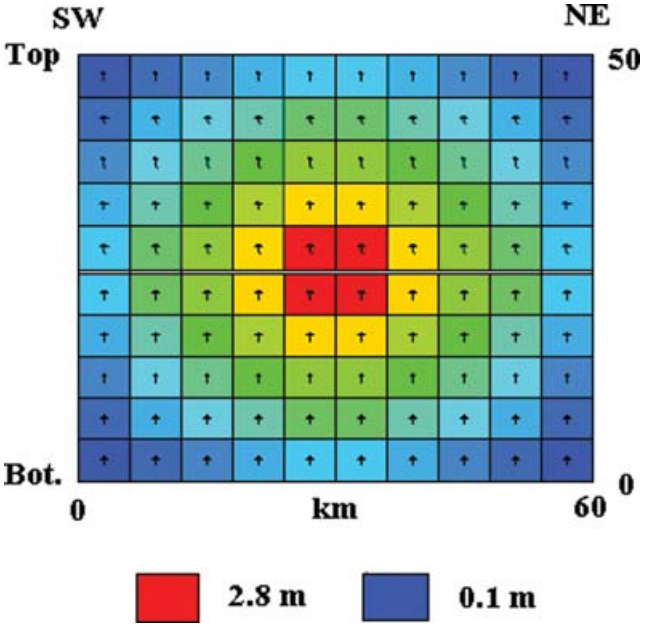

Figure 9. Tapered slip distribution for the dual-segment hinged fault system in the preferred model.

Table 6. Percentages of hypocentres in regions of positive changes in CFS for the preferred model and variations of it.

	Percentage in positive region
Preferred model (Table 5)	95.2
Uniform slip	43.1
Coefficient of friction = 0.4	73.5
Initial pore pressure = 0	95.2
Initial pore pressure = Lithostatic	95.2
Segement strike + 10°	95.0
Segment strike − 10°	93.8
Segment dips + 10°	84.8
Segment dips − 10°	98.0
σ1azimuth + 10°	95.9
σ1azimuth − 10°	95.2
σ1dip + 10°	96.2
σ1dip − 10°	95.0
Top + 5 km	63.3
Top − 5 km	98.1
Omit segment 2	90.2
Omit segment 1	88.9

at 0.42 MPa. The second section is 35 km long and extends to the north east beyond Secretary Island. It has a strike of 40°, dip of 80° and a rake of −180°. The results for this section (Fig. 10 bottom) also indicate on average a negative change in CFS of −0.55 MPa with only a small area of increased CFS confined to the shallow southern edge of the fault, peaking at 0.42 MPa. The implications of this result will be discussed below.

For comparison, we can use a source that would correspond to plane 1 of the Harvard mechanism. In contrast to the results above, most of the fault surfaces would experience a positive change in CFS for the two segments of the Alpine Fault, the averages being +0.24 MPa and +0.03 MPa.. This illustrates the importance of determining the main shock fault plane.

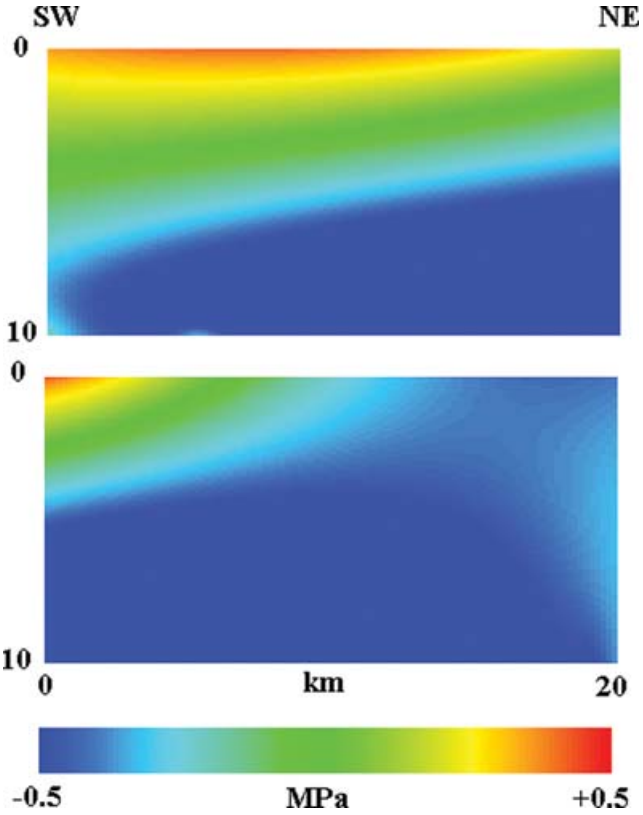

Figure 10. Changes in CFS induced by our preferred fault plane system of the 2003 Fiordland earthquake on the nearest two offshore section of the Alpine Fault. The view is of a projection on each section of the Alpine Fault itself. Top: Shows the first section that is 20 km long and parallels most of the length of Secretary Island. Here most of the fault experiences a negative change in CFS (average −0.4 MPa) with increases mainly confined to shallow depths of a few km (peaking at 0.4 MPa). Bottom: Shows the second section that is 35 km long and extends to the north east beyond Secretary Island. Here almost all the fault experiences a negative change in CFS (average −0.6 MPa) with only a small area of positive change in CFS confined to the shallow southern edge of the fault (peaking at 0.4 MPa).

DISCUSSION AND CONCLUSIONS

Using data recorded by the portable seismometers, we have determined that the 2003 Fiordland earthquake probably occurred on the plate interface between the Australian and Pacific plates. The Harvard CMT solution fault plane that is consistent with low angle thrust faulting on the plate interface can explain, using static stress calculations, the unusual aftershock distribution if most of the slip occurred near the bottom, shoreward edge of the aftershocks. This result indicates that some care is needed in interpreting main shock fault positions from aftershock distributions, as previously noted by Das & Henry (2003). As can be seen here in the 2003 Fiordland earthquake case aftershocks are primarily in the subducted plate below the interface and below the first fault plane of the hinged fault model with no aftershocks under the deeper part of the hinged fault system (Fig. 8b). Our model implies that there was little aftershock activity on the main shock fault plane. Das & Henry (2003) also found that aftershocks tend to occur near the ends of main shock faults in regions of increased CFS, although there is a wide range of behaviour. Sinohara *et al.* (2004), using ocean bottom seismometers, showed that the aftershocks of the 2003 Tokachi-Oki earthquake (Mw 8.0) occurred in a diffuse pattern well away from the area of largest slip in the main shock (their Fig. 3).

Results from our regional stress inversion determined using aftershock data show that stress in the region is, on the whole, consistent with thrust faulting on faults similar to that of the second focal plane of the Harvard CMT solution, that is, thrusting on faults dipping rather steeply to the northwest. However, this type of main shock faulting could not explain the observed diffuse aftershock positions. Aftershock sequences indicating a different stress tensor orientation to that inferred from their main shock mechanisms are not uncommon in New Zealand and has been observed for the 2001 Jackson Bay earthquake sequence (McGinty *et al.* 2005) and the 1994 Arthurs Pass earthquake sequence (Robinson & McGinty 2000). Both of these earthquakes occurred at shallow depth just to the east of the on-land section of the Alpine Fault in the central South Island in the absence of the underlying subduction. It was suggested that both earthquakes occurred on very weak faults in the region due to near lithostatic-pore fluid pressure. However, in the 2003 Fiordland case it is more likely that the occurrence of the Fiordland 2003 earthquake had reactivated a set of old, weak, surface faults that had been subducted and rotated. Without the presence of such pre-existing, faults there may have been a very low rate of aftershock occurrence. This was the case for the M_W 7.1 Puysegur Trough earthquake of 2004 November 22, which produced only ∼10 small aftershocks in the following 6 months. This event was also a subduction interface earthquake, about 100 km south of New Zealand.

The slip direction for all the large shallow earthquakes that we have considered in this study, (Fiordland, 2003 M_W 7.2 depth 23 km; Doubtful Sound, 1989, M_W 6.4, depth 24 km; Secretary Island, 1993, M_W 6.8, depth 22 km; Thompson Sound, 2000, M_W 6.1, depth 18 km), have been in or near the margin normal direction. The larger margin parallel component required to match the plate convergence direction will need to be taken up with strike-slip motion of faults similar to the offshore segments of the Alpine Fault. Our suggested slip model for the 2003 Fiordland event would have on average decreased the CFS on the closest part of the Alpine Fault by 0.4 MPa (4 bars), with the deeper sections of the fault being the most destressed (−2.3 MPa). Large shallow earthquakes of the type we would expect to occur on the Alpine Fault often initiate near their base, and thus we conclude that the 2003 Fiordland earthquake has retarded rupture of the next large Alpine Fault earthquake, at least off the Fiordland coast (this says nothing about the situation further north!). Other large events nearby could have had additional effects, but they are all smaller than the 2003 event.

The occurrence of four shallow, abutting subduction related events since 1989 in a small region near Secretary Island (Fig. 1) deserves some comment. Raised coastal platforms along the Fiordland coast indicate that there have been very large ($M > 7.5$) subduction events near Secretary Island in the past, perhaps as recently as 1826 (G. Downes & K. Berryman, personal communication, 2005). The 2003 Fiordland event was not large enough to produce significant coastal uplift. Paleoseismic investigations of other subduction zones indicate that the region of fault slip in very large interface earthquakes can be reruptured by abutting smaller events within 50–100 yr, for example, following the great 1906 Columbia earthquake. This could be the case here as well, with the structural complexity near the 17° change in strike of the subduction zone at Secretary Island also contributing. At the moment this is just speculation; we hope to develop 'synthetic seismicity' models (e.g. Robinson 2004), including viscoelastic relaxation, of the central Fiordland coast to examine this question in more detail. Such a model would also address the question of stress loading of the Alpine Fault in more detail.

ACKNOWLEDGMENTS

We thank Ian Turnbull, Simon Cox, Tim O'Neill and Ken Gledhill for their help with the field deployment and data collection. We would also like to thank the Department of Conservation for permission to deploy instruments in the Fiordland National Park. This manuscript has been improved by comments from Martin Reyners, David Rhoades, the editor and two anonymous reviewers. This work was supported by the New Zealand Foundation for Research, Science and Technology. All static stress calculations in this study used the program GNStress2, available from the anonymous ftp site ftp.gns.cri.nz in directory pub/robinson/GNStress2. The program to invert *P*-wave polarites for stress tensor orientation is in directory pub/robinson/getstress_2.

REFERENCES

Barnes, P.M., Sutherland, R. & Delteil, J., 2005. Strike-slip structure and sedimentary basins of the southern Alpine Fault, Fiordland, New Zealand, *Geol. Soc. Am. Bull.,* **117,** 411–435.

Ben-Zion, Y. & Malin, P., 1991. Fault zone head waves in the San Andreas fault zone near Parkfield, California, *EOS, Trans. Am. geophys. Un.,* **71,** 1474.

Brudy, M., Zoback, D., Fuchs, K., Rummel, F. & Baumgarten, J., 1997. Estimation of the complete stress tensor to 8 km depth in the KTB scientific drill hole: implications for crustal strength, *J. geophys. Res.,* **102,** 18 453–18 475.

Davis, J.C., 1986. *Statistics and Data Analysis in Geology*, 2nd edn, pp. 335-336, John Wiley & Sons, New York.

Das, S. & Henry, C., 2003. Spatial relation between main earthquake slip and its aftershock distribution, *Rev. Geophys.,* **41,** doi:10: 1029/2002RG000119.

DeMets, C., Gordon, R.G., Argus, D.F. & Stein, S., 1994. Effects of recent revisions to the geomagnetic reversal time scale on estimates of current plate motions, *Geophys. Res. Lett.,* **21,** 2191–2194.

Eberhart-Phillips, D., 1998. Aftershock sequence parameters in New Zealand, *Bull. seism. Soc. Am.,* **88,** 1095–1097.

Eberhart-Phillips, D. & Reyners, M., 2001. A complex, young subduction zone imaged by three-dimensional seismic velocity, Fiordland, New Zealand, *Geophys. J. Int.,* **146,** 731–746.

Hancox, G.T., Cox, S.C., Turnbull, I.M. & Crozier, M.J., 2004. Landslides and other ground damage caused by the MW7.2 Fiordland earthquake of 22 August 2003, *Proceedings of the 9th Australia New Zealand Conference on Geomechanics,* Auckland, February 2004, 7 p.

Hardebeck, J. & Shearer, P., 2003. Using *S*/*P* Amplitude Ratios to Constrain the Focal Mechanisms of Small Earthquakes, *Bull. seism. Soc. Am.,* **93,** 2434–2444.

Harris, R., 1998. Introduction to special session: Stress triggers, stress shadows, and implications for seismic hazard, *J. geophys. Res.,* **103,** 24 347–24 358.

King, G. & Cocco, M., 2001. Fault interaction by elastic stress changes: New clues from earthquake sequences, *Adv. Geophys.,* **44,** 1–38.

McCloskey, J., Nalbant, S. & Steacy, S., 2005. Indonesian earthquake: earthquake risk from coseismic stress, *Nature,* **434,** 291.

McGinty, P.J., 2004. The 2003, Mw 7.2 Fiordland earthquake and its near-source aftershock strong motion data, *Bull. N. Z. Nat. Soc. Earthq. Eng.,* **37,** 139–145.

McGinty, P.J. & Robinson, R., 1999. Slip distribution of the Lake Tennyson earthquake, New Zealand, as inferred from static stress changes and off fault aftershocks, *Geophys. Res. Lett.,* **26,** 1961–1964.

McGinty, P.J., Robinson, R. & Webb, T.H., 2005. The 2001 Ml 6.2 Jackson Bay earthquake sequence, South Island, New Zealand, *N. Z. J. Geol. Geophys.,* **48,** 315–324.

Marsan, D. & Nalbant, S., 2005. Methods for measuring seismicity rate changes; a review and a study of how the Mw 7.3 Landers earthquake

affected the aftershock sequence of the Mw 6.1 Joshua Tree earthquake, *Pure appl. Geophys.,* **162,** 1151–1185.

Menke, W. & Schaff, D., 2004. Absolute earthquake locations with differential data, *Bull. seism. Soc. Am.,* **94,** 2254–2264.

Michael, A., 1987a. Use of focal mechanisms to determine stress: A control study, *J. geophys. Res.,* **92,** 357–368.

Michael, A., 1987b. Stress Rotation During the Coalinga Aftershock Sequence, *J. geophys. Res.,* **92,** 7963–7979.

Norris, R.J. & Cooper, A.F., 2001. Late Quaternary slip rates and slip partitioning on the Alpine Fault, New Zealand, *J. Struct. Geol.,* **23,** 507–520.

Okada, Y., 1992. Internal deformation due to shear and tensile faults in a half-space, *Bull. seism. Soc. Am.,* **82,** 1018–1040.

Raleigh, C., Healy, J. & Bredehoeft, 1972. Faulting and crustal strength at Rangely, Colorado. in *Flow and Fracture of Rock, Geophysical Monograph Series,* Vol. 16, pp. 275–284, eds Heard, H., Borg, I.Y., Carter, N.L. & Raleigh, C.B., GU, Washington DC.

Reyners, M. & Webb, T., 2002. Large earthquakes near Doubtful Sound, New Zealand, 1989–93, *N. Z. J. Geol. Geophys.,* **45,** 109–120.

Reyners, M., Gledhill, K. & Waters, D., 1991. Tearing of the subducted Australian plate during the Te Anau, New Zealand, earthquake of 1988 June 3, *Geophys. J. Int.,* **104,** 105–115.

Reyners, M., Robinson, R., Pancha, A. & McGinty, P., 2002. Stresses and strains in a twisted subduction zone—Fiordland, New Zealand, *Geophys. J. Int.,* **148,** 637–648.

Reyners, M. *et al.*, 2003. The MW 7.2 Fiordland earthquake of August 21, 2003: background and preliminary results, *Bull. N. Z. Nat. Soc. Earthq. Engin.,* **36,** 233–248.

Rhoades, D. & Van Dissen, R., 2003. Estimates of the time varying hazard of rupture of the Alpine Fault, New Zealand, allowing for uncertainties, *N. Z. J. Geol. Geophys.,* **46,** 479–488.

Robinson, R., 1994. Shallow subduction tectonics and fault interaction: the Weber, New Zealand, earthquake sequence of 1990–1992, *J. geophys. Res.,* **99,** 9663—9679.

Robinson, R., 2004. Potential earthquake triggering in a complex fault network: The Northern South Island, New Zealand, *Geophys. J. Int.,* **159,** 734–748.

Robinson, R. & McGinty, P., 2000: The enigma of the Arthur's Pass, New Zealand, earthquake, 2: the aftershock distribution and its relation to regional and induced stress fields, *J. geophys. Res.* **105,** 16 139–16 150.

Robinson, R. & Webb, T., 1996. AMPRAT and MECHTOOL: programmes for determining focal mechanisms of local earthquakes, *Institute of Geological &Nuclear Sciences, Science Report* 96/7, Wellington.

Robinson, R., Webb, T., McGinty, P., Cousins, J. & Eberhart-Phillips, D., 2003. The 2000 Thompson Sound Earthquake, New Zealand, *N. Z. J. Geol. Geophys.,* **46,** 331–341.

Sinohara, M. *et al.*, 2004. Aftershock Observations of the 2003 Tokachi-Oki earthquake by using dense ocean bottom seismometers, *Earth Planet. Space,* **56,** 295–300.

Stirling, M.W., McVerry, G.H. & Berryman, K.R., 2002. A new seismic hazard model for New Zealand, *Bull. seism. Soc. Am.,* **92,** 1878–1903.

Sutherland, R. *et al.*, 2007. Do great earthquakes occur on the Alpine Fault in central South Island, New Zealand, in *Tectonics of a Continental Transform Plate Boundary: The South Island, New Zealand, AGU Geophysical Monograph*, in press.

USGS, 2003. http://earthquake.usgs.gov/eqcenter/eqarchives/poster/2003/20030821.php

Waldhauser, F. & Ellsworth, W., 2000. A double-difference earthquake location algorithm: method and application to the northern Hayward fault, California, *Bull. seism. Soc. Am.,* **90,** 1353–1368.

Wells, A., Yetton, M., Duncan, R. & Stewart, G., 1999. Prehistoric dates of the most recent Alpine Fault earthquakes, New Zealand, *Geology,* **27,** 995–998.

White, S., Trenkamp, R. & Kellogg, J., 2003. Recent Crustal Deformation and the Earthquake Cycle along the Ecuador-Columbia Subduction Zone, *Earth planet. Sci. Lett.,* **216,** 231–242.